Bulletin of the Geological Society of Finland, Vol. 97, 2025, pp 91–113 https://doi.org/10.17741/bgsf/97.2.001

# Seismic attribute analysis for enhanced interpretation of the internal reflectivity within the Kevitsa Ni-Cu-PGE bearing intrusion, northern Finland

Niina Junno[1*], Emilia Koivisto[2] and Ilmo Kukkonen[2]

[1]*Institute of Seismology, Department of Geosciences and Geography, POB 68, FI-00014 University of Helsinki*

[2]*Department of Geosciences and Geography, POB 68, FI-00014 University of Helsinki*

VERTAISARVIOITU
KOLLEGIALT GRANSKAD
PEER-REVIEWED
www.tsv.fi/tunnus

## Abstract

A three-dimensional seismic reflection survey was conducted in 2010 in northern Finland over the Kevitsa mafic-ultramafic intrusion that hosts a large, disseminated Ni–Cu–PGE sulfide deposit. In the seismic data, layered subhorizontal reflections are observed within a constrained region inside the intrusion, in the vicinity of the Kevitsa resource area. In this study, we use seismic attribute analysis to study this reflectivity. Based on the attribute analysis, an earlier three-dimensional model of lithological contacts and near mine structures is validated and updated. The attribute analysis delineates the internal reflectors more precisely and reveals structures not seen in conventional amplitude displays earlier. These later structures have cut the originally continuous internal reflectors into piecewise packages. Better understanding of the spatial distribution of the reflective packages is significant for targeted mineral exploration at depth and the structures can potentially be critical for geotechnical planning of the Kevitsa open pit. We discuss a possible scenario for the genetic link between the internal reflectivity and magmatic layering, country rock contamination, hydrothermal alteration and sulfide mineralization. The existence of subhorizontal seismically reflective layers is attributed to successive magma pulses within the Kevitsa resource area, affected by country rock contamination and hydrothermal alteration. Overall, our interpretation is that the internal reflectors within the Kevitsa intrusion represent altered and possibly mineralized parts of the magma pulses.

**Keywords**: seismic reflection data; seismic interpretation; quantitative interpretation; seismic attributes; hydrothermal alteration; mineral exploration

*Corresponding author (email: niina.junno@helsinki.fi)

Editorial handling: Suvi Heinonen (email: suvi.heinonen@helsinki.fi) and Jussi S. Heinonen (email: jussi.heinonen@abo.fi)

# 1. Introduction

Seismic reflection methods have been used for mineral exploration in hard rock environments for decades (e.g., Malehmir et al. 2012a, 2015 and references therein). The reflection seismic methods are of particular interest because of their depth penetration and significantly higher resolution when compared to other geophysical methods. Over the past two decades, the advances in data acquisition and data processing have further improved the resolution of the seismic data and reduced the acquisition and processing costs, making seismic imaging more affordable (e.g., Bellefleur et al. 2019; Malehmir et al. 2020; Alcalde et al. 2022).

The common goal of reflection seismic surveying for hard rock mineral exploration is mapping structures or contacts between lithologies where ore deposits are known to accumulate (e.g., Drummond et al. 1998). Some surveys have resulted in direct detection of the ore deposits themselves (e.g., Milkereit et al. 1996; Malehmir et al. 2021). Interpretation of seismic reflection data from hard rock mineral exploration environments is often challenging due to the complex geological architecture of the target and the inherent heterogeneity of the background (e.g., L'Heureux et al. 2009). Petrophysical properties of sulfide minerals imply that they should be strong reflectors of seismic energy in typical hard rock environments and could be directly observed if the deposits meet the size, thickness, and presentation constraints required for reflection or diffraction (e.g., Salisbury et al. 2003). Although the seismic methods have been in widespread use in mineral exploration with large quantities of collected data and big developments in acquisition and processing of that data, understanding the seismic response of the ores and ore-bearing structures in these complex environments requires more attention. For example, the effect of hydrothermal alteration on the seismic properties is still poorly understood, although alteration has been interpreted in many papers to affect the seismic properties and observed reflectivity in seismic data (e.g., Chopping 2008; Heinonen et al. 2012; Miah et al. 2015; Schetselaar et al. 2019; de Souza et al. 2020; Junno et al. 2020).

The site of this study is the Kevitsa Ni-Cu-PGE -bearing intrusion in northern Finland, where high resolution 2D and 3D seismic reflection data were acquired. Initial interpretations of the Kevitsa seismic data have been presented by Malehmir et al. (2012b), Koivisto et al. (2012) and (2015). Koivisto et al. (2015) presented a 3D model of lithological contacts and near mine structures based on the Kevitsa 2D and 3D seismic data and borehole data. This model included a set of surfaces representing magmatic layering within the Kevitsa intrusion that was at the time considered a potential explanation for the internal reflectivity observed within a constrained region inside the intrusion and associated with the known resource area (Koivisto et al. 2015). Magmatic layering had been presented as potential hypothesis for the origin of Kevitsa ore deposit. These magmatic layers represented a spectrum of olivine pyroxenites with mineralization accumulating at the bases of the individual layers (Standing et al. 2009; Gregory et al. 2011). Junno et al. (2020) used data mining, namely the Self-Organizing Map (SOM) analysis, of the extensive Kevitsa borehole data and the modelling of the effect of mineralization and alteration on the reflectivity properties of Kevitsa rock types, based on average modal compositions of the rock types, to study the possible causes for the observed internal reflectivity within the Kevitsa intrusion. They suggested that the alteration and possibly associated mineralization could be potential cause for the observed reflectivity rather than lithological contacts or mineralization alone (Junno et al. 2020).

In this paper, we use seismic attribute analysis of the Kevitsa 3D seismic reflection data to further study the observed internal reflectivity within the Kevitsa intrusion. Seismic attribute analysis provides a fast, cost-effective, and efficient interpretation tool that can reveal structures not seen in conventional interpretations. It has been increasingly used to aid the interpretation efforts in hard rock environment (e.g., Stuart et al. 2000;

Manzi et al. 2012, 2013, 2020; Hale 2013; Nkosi et al. 2018; Zhang & Wang 2024). The attribute-guided interpretation of the Kevitsa 3D seismic data refines the internal reflector geometry and revises the network of near-mine structures. The later near-mine structures have cut the originally sub-horizontally continuous internal reflectors into piecewise packages. Better understanding of the spatial distribution of the reflective packages can be significant for targeted mineral exploration at depth and the structures can potentially be critical for geotechnical planning of the Kevitsa open pit. We discuss a possible scenario for the genetic link between the internal reflectivity and magmatic layering, country rock contamination, hydrothermal alteration and sulfide mineralization within the Kevitsa resource area. The existence of several sub-horizontal seismically reflective layers within a restricted region inside the Kevitsa intrusion and associated with the resource area are attributed to successive magma pulses affected by country rock contamination and hydrothermal alteration. The hydrothermal alteration may have been further aided by introduction of fluids through structures some of which are identified in this study. Overall, our interpretation is that the reflective layers represent altered and possibly mineralized (sulfide-bearing) parts of the magma pulses as also suggested by Junno et al. (2020).

# 2. Background

## *2.1. Geological setting of the Kevitsa intrusion*

Kevitsa mafic-ultramafic intrusion, dated at 2057 ± 5 Ma (Mutanen & Huhma 2001), is hosted by the Central Lapland Greenstone Belt (CLGB) that consists of Paleoproterozoic metamorphosed and hydrothermally altered volcanic and sedimentary rocks (Fig. 1). CLGB extends over an area of 100 km by 200 km and forms one of the largest Paleoproterozoic greenstone belts in the world. CLGB exhibits a complex geologic history that spans 600 Ma starting in circa 2.5 Ga and culminating in regional compressional tectonic event at around 1.9 Ga that is characterized by NE-SW-striking faults (Manninen et al. 1996; Hanski & Huhma 2005). It consists of several lithostratigraphic units: Salla, Kuusamo, Sodankylä, Savukoski, Kittilä and Kumpu groups described in detail in e.g., Hanski & Huhma (2005) and revised by Huhma et al. (2018). CLGB represents different and relatively complex metamorphic history. The younger north-northwestern part of the belt has experienced greenschist facies metamorphism, whereas towards the older east-southeastern part of the belt the degree of metamorphism increases rather abruptly to amphibolite facies (Hanski & Huhma 2005).

CLGB hosts many differentiated, mafic-ultramafic bodies and mafic dykes, some of which host notable ore deposits, that were emplaced on CLGB rocks in several stages (Hanski et al. 2001; Huhma et al. 2018). The Kevitsa-Satovaara intrusive complex consists of two separate intrusions, Kevitsa and Satovaara that are suggested to be originally formed as a single intrusive body that was later separated by north-east trending faults (Hanski & Huhma 2005). Satovaara intrusion has been displaced southeastward, approximately 2–3 km, in relation to Kevitsa intrusion (Mutanen 1997, 2005). Both intrusions are hosted by phyllites and black schists within the Savukoski group of CLGB. Satovaara intrusion hosts a disseminated Ni-Cu-PGE-Au deposit, similar to the Kevitsa deposit, but the exploration studies conducted by Geological Survey of Finland in 1995 were not promising in terms of mining the deposits (Mutanen 1997, 2005).

Kevitsa intrusion consists of gabbroic rocks in the southwest and olivine pyroxenite and its variants in the northeast (Fig. 1). Several (probably) older dunite units are found within and around the intrusion (e.g., Central Dunite in Fig. 1 and 2). These dunite units may have played a role in the larger scale emplacement of the Kevitsa intrusion and possibly also in the formation of the disseminated mineralization (e.g., Luolavirta et

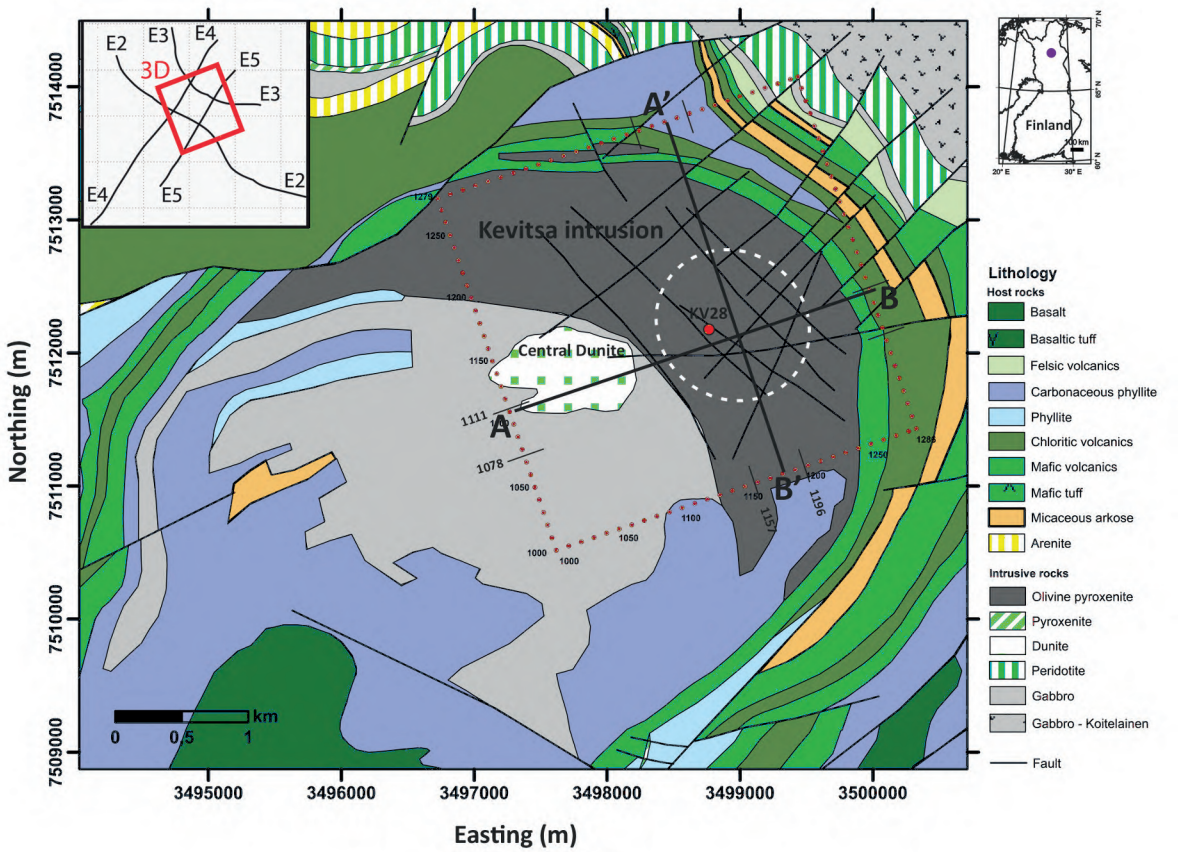


**Figure 1.** Geological map of the Kevitsa intrusion. The Kevitsa intrusion consist mainly of olivine pyroxenite shown in dark grey and gabbro in light grey. Central Dunite unit sits within the intrusion. The 3D seismic survey area is shown with dashed red square and the approximate location of the resource area in white dashed oval. The location of the borehole KV28 indicated with red dot. The index map shows the location of the 2D seismic survey lines in relation to the 3D survey area. The A-B (crossline 1110) and A'-B' (inline 1180) indicate the cross-sections of the 3D seismic data cube shown in Fig. 2 and 3. The location for inlines 1157 (Fig. 7 and 9) and 1196 (Fig. 5) and crosslines 1078 (Fig. 6) and 1111 (Fig. 8) are shown on the map. Geology adapted from a map provided by First Quantum Minerals Ltd.

al. 2018a). At the surface, the roughly oval-shaped Kevitsa intrusion covers an area of about 16 km$^2$ (Mutanen 1997), and it reaches about 1.5 km depth at its deepest parts (Koivisto et al. 2012, 2015). The southern and northern margins of the intrusion show undeformed contacts with the hosting CLGB rocks (Standing et al. 2009). The southeastern margin of the Kevitsa intrusion is cut by major steeply NE-dipping Satovaara fault zone. The intrusion is overprinted by several structures that developed during the evolution of the Satovaara fault zone (Lindqvist et al. 2017). Lindqvist et al. (2017) defined three major orientations of fracture zones: i) gently WNW-dipping, ii) moderately to steeply SE-dipping, and iii) sub-vertical NNW-striking zones that are also recognized in the 3D seismic reflection data. These structures intersect the deeper parts of the Kevitsa mine plan which highlights the significance of these structures to mine stability (Koivisto et al. 2015). The gently WNW-dipping structures have the largest lateral and vertical extents and are critical feature for the slope stability in the open pit (Lindqvist et al. 2017). The moderately to steeply SE-dipping zones have large vertical extents and occur in the northern part of the pit. The sub-vertical NNW-striking zones

have variable dips towards both east and west and show no clear one-to-one continuity from pit-depth models into the deeper seismic models. In addition, Lindqvist et al. (2017) identified a NW-striking structures that have both the moderately NE- and steeply SW-dipping orientations. These structures were considered critical for pit stability since most of these features are in near vicinity of the open pit main ramp.

Hydrothermal alteration is notable throughout the Kevitsa deposit and the hosting intrusion (e.g., Santaguida et al. 2015). Several different alteration styles have been identified in Kevitsa, the main alteration styles being amphibole, serpentine, and epidote alteration (Le Vaillant et al. 2016). Amphibole alteration is the most recognizable and widespread of the alteration styles within the Kevitsa area. This amphibole alteration consists of replacement of clinopyroxene by tremolite-actinolite and orthopyroxene by cummingtonite-grunerite (Le Vaillant et al. 2016). The pervasive, partial serpentine alteration of olivine in peridotitic rocks appears to be the first alteration event in Kevitsa. Alteration of pyroxene and olivine is intense in places, which makes the identification of the primary rock types difficult. The amphibole and serpentine alteration styles are spread throughout the Kevitsa intrusion, and they enclose decimeter-scale patches of essentially fresh igneous rock (Le Vaillant et al. 2016). The epidote alteration is structurally controlled and associated with NE-trending faults cutting across the Kevitsa deposit (Le Vaillant et al. 2016). Talc and carbonate alteration is also observed associated with late fractures and veins (Pittuck & Lepley 2019). This alteration style occurs notably beneath the Kevitsa deposit, within and around a flat-lying shear zone and composite quartz-carbonate vein (Pittuck & Lepley 2019).

Kevitsa deposit was found in 1987 (Mutanen 1997). Kevitsa is one of Finland's largest open-pit mines and one of Finland's largest mineral discoveries (Boliden 2024). Open-pit mining commenced in 2012 by First Quantum Minerals Ltd and in June 2016 Boliden AB acquired the mine. In 2023, the mined-out ore tonnage was 9.405 Mt (Berthet 2024) with the main metals being copper, nickel, palladium, platinum, gold, and cobalt. Cu is the most valuable commodity in Kevitsa (Berthet 2024). The mineral resources in Kevitsa are 0.34% Cu, 0.23% NiS, 0.17 ppm Pt, 0.11 ppm Pd, 0.09 ppm Au, and 0.01% CoS (Berthet 2024). Currently, the mining in Kevitsa is planned to continue until 2033 with planned final pit depth of about 550 m (Boliden 2024).

In the Kevitsa intrusion, the economic mineralization occurs in compositionally heterogeneous olivine pyroxenites, whereas more homogeneous olivine pyroxenites occur outside the Kevitsa resource area (Standing et al. 2009; Gregory et al. 2011). Mutanen (1997) first studied the Kevitsa intrusion and associated deposits. According to Mutanen (1997), the Kevitsa intrusion formed as a single cast of magma and the heterogeneities of the ultramafic complex reflect variable degrees of in-situ crustal contamination. The main mineralization was interpreted to occur as continuous bodies extending up to hundreds of meters in diameter (Mutanen 1997). Mutanen (1997) attributes the origin of sulfur to host rock contamination that took place by incorporating metasedimentary material in the ultramafic magma as it intruded the bedrock. Thereafter, several genetic models have been presented for the evolution of the Kevitsa intrusive complex and the formation of the Kevitsa ore deposit. Gervilla & Kojonen (2002) considered that hydrothermal alteration has been contributing to the formation of the Ni-PGE ore at the Kevitsa deposit, although others (e.g., Santaguida et al. 2015; Le Vaillant et al. 2016) have argued against this theory stating that the alteration processes did not affect the Ni and PGE grades. Gervilla & Kojonen (2002) argued that the low-grade disseminated ore was upgraded by alteration and metamorphism. Re-mobilization of Ni and PGE took place via hydrothermal and metamorphic fluids that also redistributed the S and Cu in sulfides. Lamberg et al. (2005) present that the PGE rich zones show alteration and argued that the ore material was enriched with precious metals in the staging magma reservoir and as the

magma penetrated upwards, it encountered the Kevitsa cumulates and became even more enriched with Ni. According to the model by Yang et al. (2013), the initial komatiitic magma intruded and interacted with sulfide rich black shale triggering sulfide saturation which in turn interacted with Ni-rich magma resulting in high Ni-tenor of the sulfides. Yang et al. (2013) proposed that initially some semi-massive or massive Ni-rich sulfides may have been accumulated from this initial komatiitic magma, but they were picked up and broke down by ascending Kevitsa basaltic magma that intruded through the same magma conduit. This resulted in enrichment of Ni in the basaltic magma and formation of high Ni-PGE ore from the Ni rich magma and the regular ore with normal Ni content further away. Standing et al. (2009), Gregory et al. (2011), and Koivisto et al. (2015) presented a model involving several magma emplacements on top of each other forming layers of differentiated olivine pyroxenites. The magmatic layers were suggested to represent a spectrum of olivine pyroxenites ranging from plagioclase- and orthopyroxene-rich tops (plagioclase-bearing olivine websterite) to increasing percentages of olivine and clinopyroxene (olivine pyroxenite) towards the bottoms of the layers. The magmatic layers were inferred to control the extent of the economic mineralization, with sulfides concentrated at the bottoms of the layers (Standing et al. 2009; Gregory et al. 2011). Le Vaillant et al. (2016, 2017) and Luolavirta et al. (2018b, 2018c) interpret the resource area in Kevitsa to be associated with a local development of cyclic units that generally lack obvious internal layering. The magmas producing the Ni-PGE rich ores are considered to have likely passed through distinct country rocks and followed a different route into the Kevitsa magma chamber (Luolavirta et al. 2018c). Le Vaillant et al. (2016) considered the hydrothermal alteration and concluded that it has little importance in the generation of mineralization in Kevitsa. However, Le Vaillant et al. (2016) suggest that Cu and Au grades may have been affected by remobilization from centimeter to kilometer scale.

## 2.2. Earlier seismic reflection studies in Kevitsa

As part of the HIRE project (High-Resolution Reflection Seismics for Ore Exploration 2007–2010) four intersecting 2D seismic reflection profiles (E2, E3, E4 and E5 on the index map in Fig. 1) were acquired at Kevitsa in 2007 (Kukkonen et al. 2009). Koivisto et al. (2012) provided a detailed description of the 2D seismic reflection data acquisition, processing, as well as initial interpretation. Koivisto et al. (2012) used the 2D seismic reflection data to establish the shape and extent of the Kevitsa intrusion, thus providing an overall framework for future exploration in the area. The Kevitsa deposit was noted to locate within a part of the intrusion associated with distinct, gently dipping reflectivity characteristics. The 2D seismic data also revealed a complex pattern of faults, in particular a series of major fault and shear zones bracketing and crosscutting the Kevitsa intrusion. A 3D seismic reflection survey was conducted in 2010 in Kevitsa (Fig. 1), primarily for mine planning but also for deep mineral exploration purposes. The 3D seismic survey is limited to the closer vicinity of the known deposit, while the 2D seismic survey was designed to provide a more regional view of the Kevitsa intrusive complex. Malehmir et al. (2012b) provided a detailed description of the 3D seismic reflection data acquisition, processing, and initial interpretation. The 3D reflection data showed short, gently dipping high-amplitude reflections within a constrained area inside the intrusion and in the vicinity of the Kevitsa resource area. These reflections were at the time interpreted to originate from internal magmatic layering within the Kevitsa main intrusion. Steeply dipping faults were observed as time shifts or phase changes along the gently dipping reflections forming a complex reflection pattern. Some of the interpreted faults cross the planned open-pit mine at depths of about 300–500 m and most likely continue to the surface above the depth of the seismic imaging capability, and are, therefore, critical for geotechnical planning of the open pit.

Some of the major structures identified in the seismic sections may potentially be related to the emplacement of the Kevitsa intrusion (Malehmir et al. 2014).

A vertical seismic profiling (VSP) survey was conducted in borehole KV28 prior to the 3D survey to provide information about the near-vertical structures (Malehmir et al. 2012b). KV28 which was at the time the deepest borehole at the location of the planned open pit (Fig. 1). The direct down going P-wave arrivals from the VSP survey were used to check the consistency (along with available sonic logs) of the 1D velocity function used for the migration and time-to-depth conversion of the 2D and 3D seismic reflection data (see the details in Malehmir et al. 2012b and Koivisto et al. 2012). The 1D velocity model is an approximate root-mean square-velocity function that was derived from the velocity analysis of both the 2D and 3D seismic data by obtaining the optimal stacking velocity function for approximately horizontal reflectors (Koivisto et al. 2012; Malehmir et al. 2012b; Koivisto et al. 2015). The same time-to-depth conversion was used for both the 2D and 3D seismic data. Accurate time-to-depth conversion is crucial for the determination of reliable depth of interpreted features in the seismic data. Generally, the seismic velocities of the Kevitsa rock types vary quite a bit (e.g. within 6400 m/s and 7200 m/s for olivine pyroxenite variants, see details in Junno et al. 2020 Fig. 4). However, based on systematic comparison of the seismic reflections with the known contacts in the boreholes by Koivisto et al. (2015), this 1D velocity model is representative of the whole intrusion, with typical differences between the contacts in the boreholes and in the seismic data in further parts of the Kevitsa intrusion within just a couple of meters (e.g. see Fig. 8 in Koivisto et al. 2015). Within the Kevitsa resource area, the accuracy of the 1D velocity model can be considered very good.

In the earlier studies (Malehmir et al. 2012b, 2014; Koivisto et al. 2012, 2015), laterally continuous reflections were observed in the Kevitsa 2D and 3D seismic reflection data within a limited region inside the intrusion from about 200–300 m to about 1 km depth. This reflectivity was interpreted to be associated with the extent of the economic mineralization (Fig. 2). Koivisto et al. (2015) suggested that the laterally continuous internal reflectivity within the Kevitsa intrusion originates from smaller-scale magmatic layering controlling the extent of the main economic mineralization, as was proposed to explain the Kevitsa ore genesis by Standing et al. (2009) and Gregory et al. (2011) at the time of the seismic surveys. On average, the contrast between the physical properties of plagioclase-bearing olivine websterite, the tops of the magma pulses, and olivine pyroxenite, the bottoms, was found to be enough to produce detectable reflections. However, Koivisto et al. (2015) noted that this explanation for the internal seismic reflectivity was not unequivocally supported by the borehole data, mainly due to varying lithological logging practices over the years.

Junno et al. (2020) used data mining, namely Self-Organizing Map analysis, of the extensive Kevitsa borehole data and the modelling of the effect of mineralization and alteration on the reflectivity properties of Kevitsa rock types, based on average modal compositions of the rock types, to further study the possible causes for the observed internal reflectivity within the Kevitsa intrusion. They suggested that the seismic reflectivity can possibly be attributed to alteration and may also be linked to the presence of mineralization, although higher sulfide content was not seismically required as the alteration alone could cause observable reflections. The interpretation by Junno et al. (2020) would also require that the altered (and possibly mineralized) zones are somewhat layered. This would imply that the observed reflectivity might originate from altered (and possibly mineralized) magma pulses, or altered parts of the magma pulses, in contact with less altered (unmineralized) parts of the intrusion.

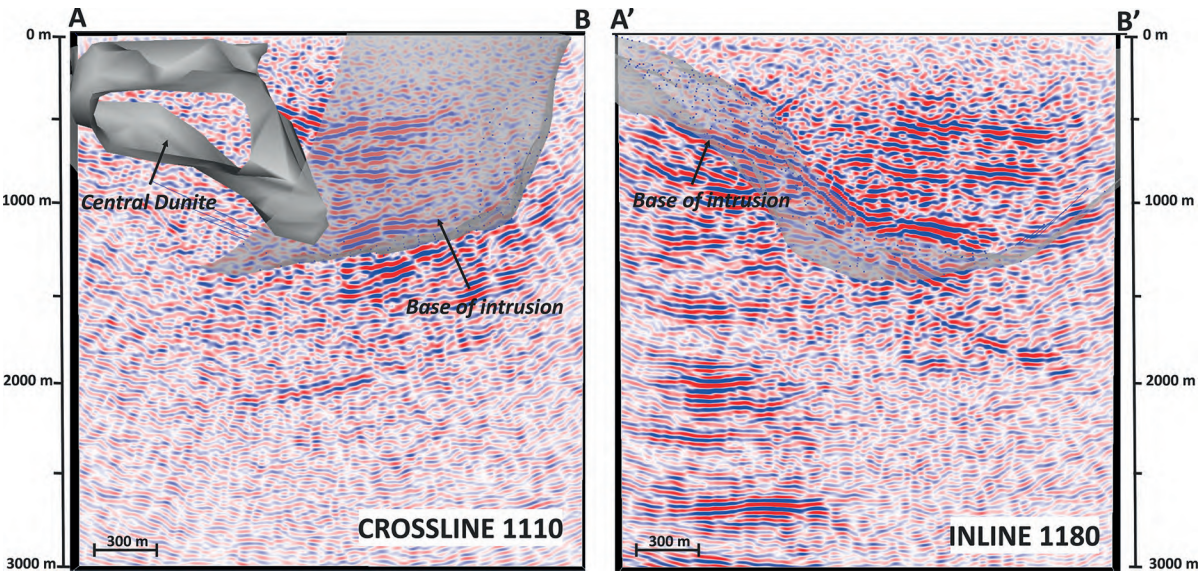


**Figure 2.** Internal reflectivity within the Kevitsa intrusion, see location for A-B and A'-B' in Fig. 1. Cross-section A-B correspond to crossline 1110 of the 3D seismic data (migrated; Malehmir et al. 2012b) and A'-B' correspond to inline 1180. The base of the Kevitsa intrusion and the Central Dunite body (Koivisto et al. 2015) are shown as reference. The depth is referenced to the datum level of the 3D seismic reflection data (at 290 m above sea level).

## 2.3. *Initial 3D model of the lithological contacts and near mine structures*

Koivisto et al. (2015) built and presented a 3D model of geological contacts and near-mine structures using the 2D and 3D reflection seismic data together with the borehole data and geological maps of the Kevitsa area. The 3D lithological model consists of surfaces that represent contacts between lithological units. The key features of the model are the base of the Kevitsa intrusion and its previously unknown south-southwestern continuation, smaller-scale magmatic layering within the intrusion, several host rock units surrounding the intrusion, as well as the Central dunite unit and the top and bottom of the footwall dunite unit (see details in Koivisto et al. 2015). The surfaces for the lithological contacts are more strictly based on the 3D seismic reflection data as the 3D data record the true geometry of the reflectors more reliably. However, the 2D data covers larger area, and thus some of the surfaces are only based on the 2D seismic reflection data (such as the top and bottom of the southern continuation of the Kevitsa main intrusion that lies outside the 3D seismic data cube; Koivisto et al. 2015). In addition to 2D and 3D seismic reflection data, the modelled surfaces have been fitted to known contacts in the borehole data and in some cases to surface geological map. Discrete smooth interpolation method by Mallet (1997) was used to create surfaces from the picked control points (see details in Koivisto et al. 2015).

The 3D model of near-mine structures consists of surfaces that are fitted to persistent breaks and offsets in the reflections that have been interpreted as prevailing structures in the 3D seismic data (Koivisto et al. 2015). Occasionally, parts of the interpreted structures were found reflective, such as the gently WNW-dipping continuous reflector called R8 which is also the shallowest feature interpreted in the 3D seismic data (150 meters below the surface) and it appears to provide a boundary to the internal reflectivity within the Kevitsa intrusion (Koivisto et al. 2015). R8 has

been suggested to also represent a major structure that is critical for the slope stability in the open pit (e.g., Lindqvist et al. 2017; Malehmir et al. 2018). The 3D model of the near-mine structures by Koivisto et al. (2015) consists of 20 surfaces that represent larger discontinuities and breaks in the inline (ten surfaces) and crossline (ten surfaces) directions. In addition, within the planned open pit, closer attention was paid to the smaller scale discontinuities which resulted in eight surfaces representing near-vertical structures. Seven of these near-vertical structures are picked in the crossline direction and only one in the inline direction. The requirement for the modeled structure was that the discontinuity had to be followed over several inlines or crosslines (generally at least ten; picked from every three sections), and the picking was terminated when it became uncertain as to pick any specific continuation (Koivisto et al. 2015).

# 3. Seismic attribute analysis

Seismic interpretation is the determination of the geological significance of the seismic data which conventionally implies picking and tracking laterally consistent seismic reflections for the purpose of mapping geologic structures (such as lithological contacts, faults etc.). The correctness of interpretation can be tested with drilling data, models derived from geophysical data or after excavation has revealed the subsurface geology in detail. Seismic attribute analysis provides a quantitative tool for interpretation, even if ultimate interpretation remains to be based on qualitative subjective assessment. However, attribute analysis provides quantitative products to aid the qualitative interpretation and help interpreter to visualize different features within the data. Seismic attributes can be used to extract information from the seismic data, and they have become an additional tool in interpretation of seismic data in hard rock environments (e.g., Stuart et al. 2000; Manzi et al. 2012, 2013, 2020; Hale 2013; Nkosi et al. 2018; Zhang & Wang 2024).

## *3.1. Mathematical background of the seismic attribute analysis*

Seismic attributes are defined as mathematical permutations, algorithms or observable features that can segment, filter, classify or describe the seismic waveform (e.g., Dewett et al. 2021). The principal objectives of the attributes are to provide accurate and detailed information on structural, stratigraphic, and lithological parameters for the seismic interpretation (Taner 2001). Seismic attributes were introduced in 1970s as useful displays to help interpretation of seismic data in a qualitative way. In this study, we use the attributes defined and classified by Taner et al. (1979) and Taner (2001), namely the instantaneous envelope, first and second envelope derivative and acoustic impedance. Each seismic attribute is defined to highlight a specific property of the seismic data. The attributes are derived from complex seismic trace CT(t) defined by Taner et al. (1979) as

$$CT(t) = T(t) + iH(t)$$

where T(t) is the seismic trace and H(t) the Hilbert transform of that seismic trace.

The instantaneous envelope or amplitude envelope is a physical attribute that represents the acoustic impedance contrast of the subsurface and hence the reflectivity. It is calculated from the complex seismic trace using the formula

$$E(t) = SQRT\,[T2(t) + H2(t)]$$

where E(t) is the envelope (Taner et al. 1979). The envelope is useful for example in highlighting discontinuities, changes in lithology and faults. Faults in the envelope attribute are usually characterized by laterally discontinuous features. This attribute is also useful for identifying major changes in lithology and bright spots. The advantage of using the instantaneous envelope instead of the original seismic trace values, such as amplitude, is that it is independent of the phase or polarity of

the seismic data, both of which affect the apparent brightness of a reflection.

First envelope derivative (DE(t)) is the change in the envelope over time (Taner et al. 1979), i.e.,

$$DE(t) = dE(t)/dt$$

It indicates sharp interfaces, such as fracturing and changes in reflectivity. The second envelope derivative (DDE(t); Taner et al. 1979))

$$DDE(t) = d2E(t)/dt^2$$

provides the measure of the sharpness of the envelope peak and is used to identify reflective interfaces within the seismic section indicating sharp changes in lithology. Relative acoustic impedance attribute is an indicator of impedance change, in a relative sense. Acoustic impedance (Z) is the product of seismic velocity (V) and density (ρ)

$$Z=V*\rho$$

The greater the difference in the acoustic impedance is the stronger reflection will result from it. The reflection coefficient (R), i.e., the ratio of reflected to incident energy, is in the simplest case of vertical incidence between upper (u) and lower (l) medium is

$$R = \frac{(Z_l - Z_u)}{(Z_l + Z_u)}$$

Generally, a reflection coefficient of 6% is thought to be enough for a detectable reflection (Salisbury et al. 2003).

## 3.2. Seismic attribute analysis of the Kevitsa 3D seismic reflection data

Seismic attribute analysis was conducted using Paradigm GOCAD and Mira Geoscience Ltd. GOCAD Mining Suite. Seismic attributes were calculated on migrated and time-to-depth converted 3D seismic reflection data. Malehmir et al. (2012b) have provided a detailed description of the original data processing. The processing followed conventional seismic reflection data processing with prestack dip-moveout and poststack migration that have been successfully used in the past for imaging complex structures in hard rock mining and exploration environments (e.g., Adam et al. 2003; Malehmir & Bellefleur 2009). Some key processing steps included careful refraction statics, velocity analysis, and prestack and poststack noise attenuations using various filtering and deconvolution approaches (see Malehmir et al. 2012b Table 2 for details, and Malehmir et al. 2018 for further discussion). The 3D seismic data processing was also done carefully to preserve the relative amplitude variations in the data. No automatic gain control or semblance filtering were used during the processing (see Malehmir et al. 2012b Fig. 6 and Table 2 for details), providing a good starting point for the attribute analysis. However, it should be noted that the interpretation presented in this paper is mainly based on analyzing the continuity of the reflectivity and the breaks in this reflectivity, not on the amplitude strength or variations within the data. The 3D seismic data processing revealed many prominent reflections within the 3D seismic volume (Malehmir et al. 2012b, 2014, 2018; Koivisto et al. 2015). However, due to the survey parameters (see Table 1 in Malehmir et al. 2012b) and high seismic velocities of the Kevitsa rock types, near-surface is under-sampled (and low fold) for reflection seismic imaging. The signal quality is poor within the first couple of hundred meters of the 3D reflection volume (Malehmir et al. 2012b). Malehmir et al. (2018) complemented the 3D reflection seismic data processing results with the results from 3D first-arrival tomography that provided insights on the near surface reflectivity allowing the linkage between the near-surface geologic features with those interpreted from the 3D seismic reflection volume.

Seismic attributes were computed in Paradigm GOCAD using the built-in algorithms from the seismic amplitude data within the 3D seismic

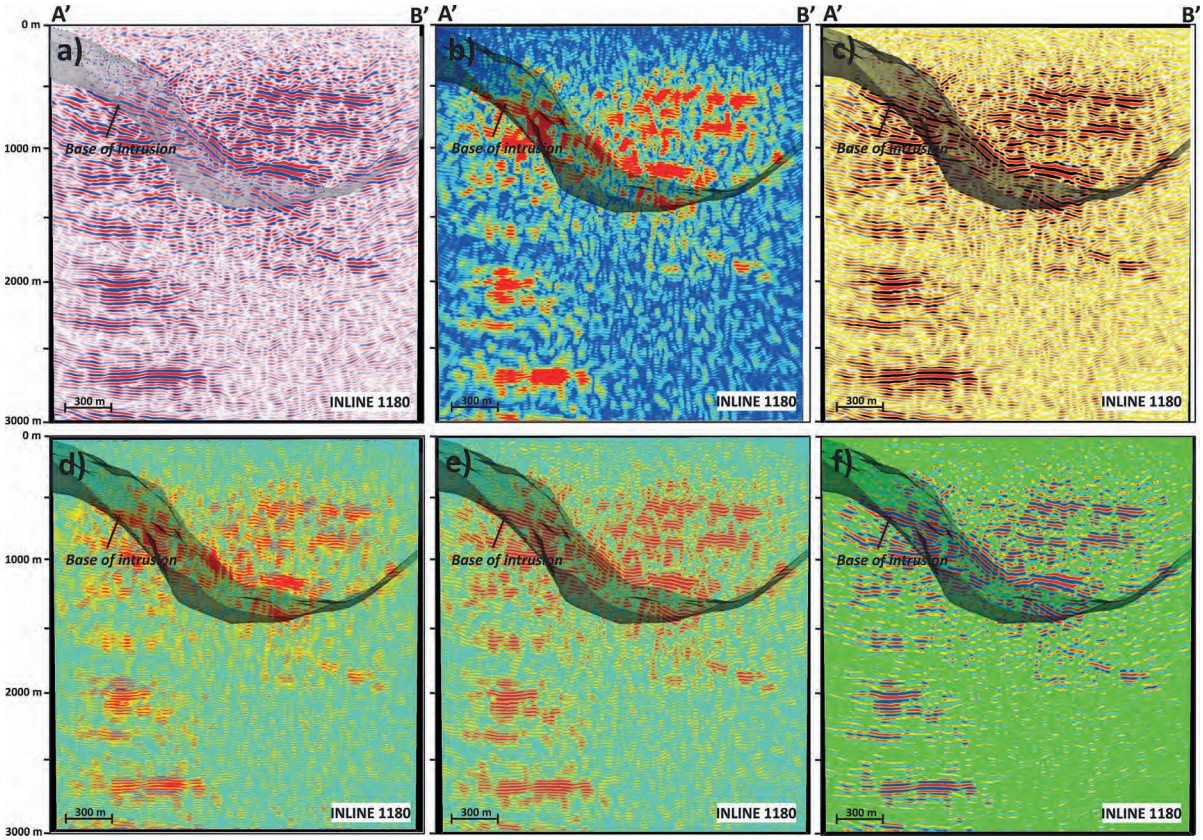


**Figure 3.** a) Seismic amplitude, b) amplitude envelope attribute, c) Hilbert transform, d) first derivative of the amplitude envelope attribute, e) second derivative of the amplitude envelope attribute, and f) relative impedance attribute of the 3D seismic data. See location for A'-B' corresponding to inline 1180 in Fig. 1. The depth is referenced to the datum level of the 3D seismic reflection data (at 290 m above sea level).

volume. Seismic data is generally stored as a 3D regular cube and each vertical column of the cube is a regular sampling of the initially continuous seismic signal (in this case the original sampling interval of the 3D data was 1 ms, which was after the time-to-depth conversion resampled to 1 m for the 3D cube that was imported into GOCAD). Representation of the continuous signal has to be rebuilt to compute seismic attributes. In GOCAD, the continuous signal is approximated using trigonometric polynomials (see details in Labrunye 2004) whose coefficients are computed using a vertical window of $2n+1$ samples. The instantaneous attributes are then calculated from the rebuilt seismic signal and the Hilbert transform using this moving window along each of the seismic traces. Based on testing of different values for $n$, $n$=10 was taken to provide the best visual representation for the interpretation (corresponding to 21 samples and 21 m). However, the consistency of the final interpretation results was checked for a range of values of $n$ ($n$=5 to 20) to make sure that only the most reliable features were included in the final set of interpreted features.

The comparison between different attributes is shown in Fig. 3. The section shown in Fig. 3 corresponds to inline 1180 denoted as A'-B' in Fig. 1. Fig. 3 compares six different attributes – a) seismic amplitude, b) amplitude envelope, c) Hilbert transform, d) first envelope derivative, e) second envelope derivative, and f) relative acoustic impedance attributes. In principle, the same reflections can be seen in all different attribute displays. Reflectivity within the intrusion

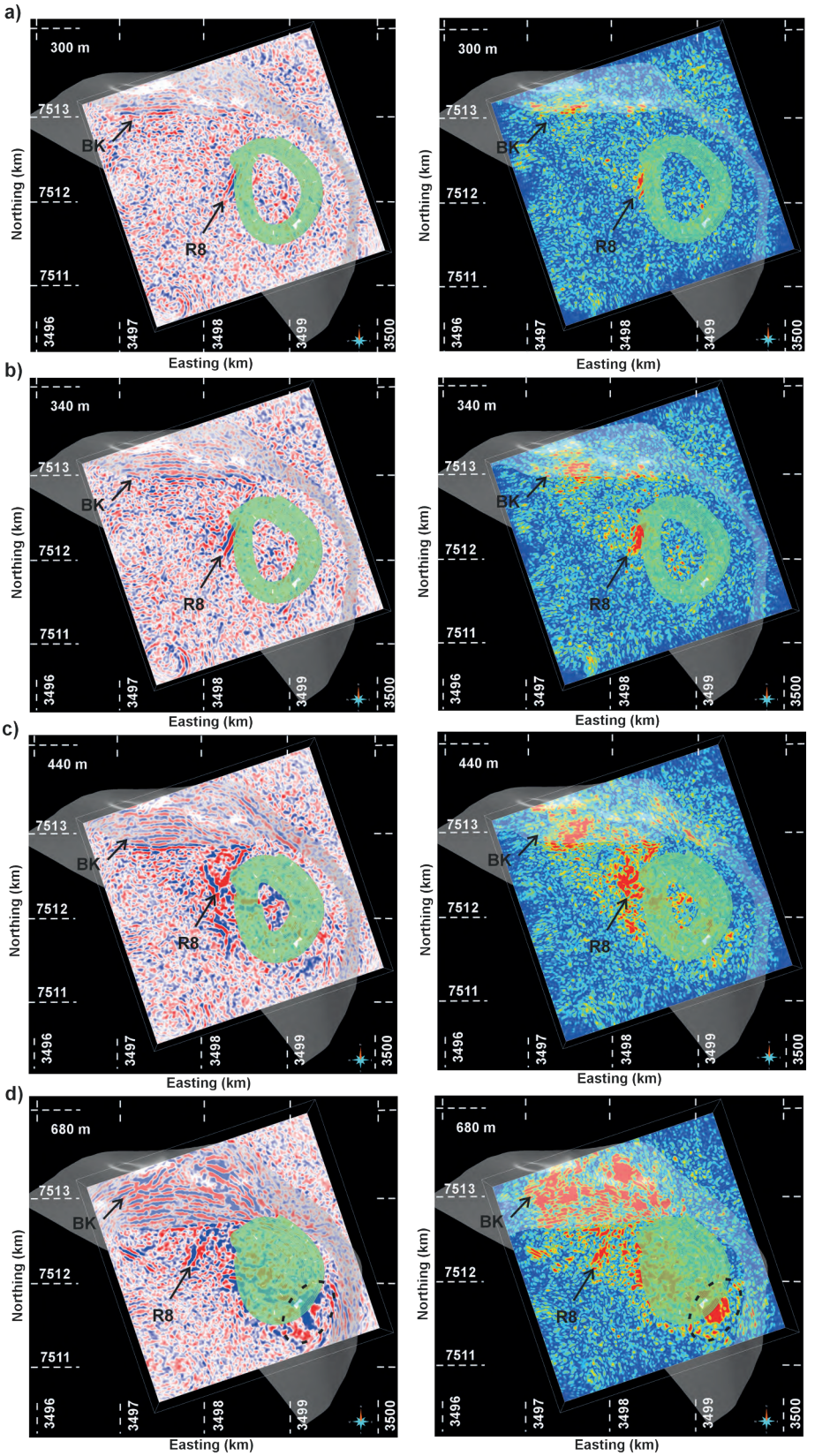


**Figure 4**. Series of depth slices in seismic amplitude (left) and amplitude envelope attribute display (right) at a) 300 m, b) 340 m, c) 440 m, and d) 680 m depth. The depth is referenced to the datum level of the 3D seismic reflection data (at 290 m above sea level). Intrusion contact is clearly visible in both attribute displays (BK in the base of the Kevitsa intrusion modelled by Koivisto et al. (2015)). Reflector R8 is the only major reflector that cuts the planned open pit (green) at its western margin. Black dashed circle indicates the location of the seismic target identified by Malehmir et al. (2018) as a bright spot anomaly that relates to layered-based sulfide mineralization. Figure is based on Malehmir et al. (2012b) and (2018).

is observed as packages of reflections rather than continuous single reflections, as also noted earlier (e.g., Malehmir et al. 2012b; Koivisto et al. 2012, 2015; Junno et al. 2020). However, the reflective packages seem less continuous in the amplitude envelope display (Fig. 3b), and especially in first and second derivatives of the envelope (Fig. 3d and 3e, respectively) than in the amplitude display (Fig. 3a). The reflective packages have clearer breaks in between and it seems that the reflectivity consists of several packages of reflections rather than one continuous reflector. These seismic attributes are useful in highlighting discontinuities and faults and sharp changes in reflectivity that indicates change in lithologies or fracturing. In addition, these attributes highlight the relative changes in physical properties of the subsurface that could indicate alteration within the subsurface. The relative acoustic impedance attribute of the 3D seismic data is presented in Fig. 3f. This attribute shows similar features as the other attribute displays in Fig. 3. The clear breaks between the reflective packages are visible, indicating possible faulting. These discontinuities could, therefore, indicate faulting within the Kevitsa intrusion.

Fig. 4 represents the series of depth slices in seismic amplitude and amplitude envelope display at depths of a) 300 m, b) 340 m, c) 440 m, and d) 680 m. The depth is referenced to the datum level of the 3D seismic reflection data (at 290 m above sea level). This figure and the depth levels are based on those used as examples in Malehmir et al. (2012b) and (2018). The observed reflectivity within the 3D seismic data starts only at the depth of approximately 300 m due to poor signal quality at the shallower depths (Malehmir et al. 2012b; Koivisto et al. 2015). The internal reflectivity is observed from about 300 m to about 1 km depth (Fig. 2). The amplitude envelope attribute is useful for identifying major changes in lithology and bright spots. The contact of the intrusion to the hosting Paleoproterozoic metamorphosed and hydrothermally altered volcanic and sedimentary rocks of the CLGB is clearly visible in both attribute displays. Reflector R8 is the only major reflector that cuts the planned open pit at its western margin, and it is also clearly visible in both attribute displays. The bright spot anomaly observed in Fig. 4d at depth of 680 m depth is more precise and constrained in amplitude envelope display than in original seismic amplitude display. This seismic target as stated in Malehmir et al. (2018) was pointed out to possibly relate to a sulfide mineralization. This target was later drilled, and it turned out not to be of economic significance.

# 4. Updated 3D model of the near mine structures

Based on the seismic attribute analysis, the 3D model of the near mine structures by Koivisto et al. (2015) was updated. The criterion by Koivisto et al. (2015) is used to update the model of the near mine (near vertical) structures presented in this paper (see chapter 2.3). The observed discontinuities in reflectivity were interpreted to represent these near vertical structures. The requirement for the modeled structure was that the discontinuity in reflectivity had to be followed over several (generally at least ten) inlines or crosslines. The picking was terminated once the continuation of the feature became unsure or ambiguous. Generally, the modelled surfaces terminate at 200–300 m depth due to poor signal quality at shallower depths (Malehmir et al. 2012b; Koivisto et al. 2015). However, in the amplitude envelope display of the 3D seismic data, the discontinuities seem to continue to shallower depths than in the seismic amplitude display (e.g., Fig. 5). The surfaces of the updated model of the near mine structures are created from the control points picked on the 3D seismic data using the discrete smooth interpolation method by Mallet (1997), as in the model by Koivisto et al. (2015) presented above.

The earlier 3D model near mine structures by Koivisto et al. (2015) consisted of 20 surfaces that represented larger discontinuities within the intrusion and eight surfaces that represented smaller-scale, near-vertical structures. The larger

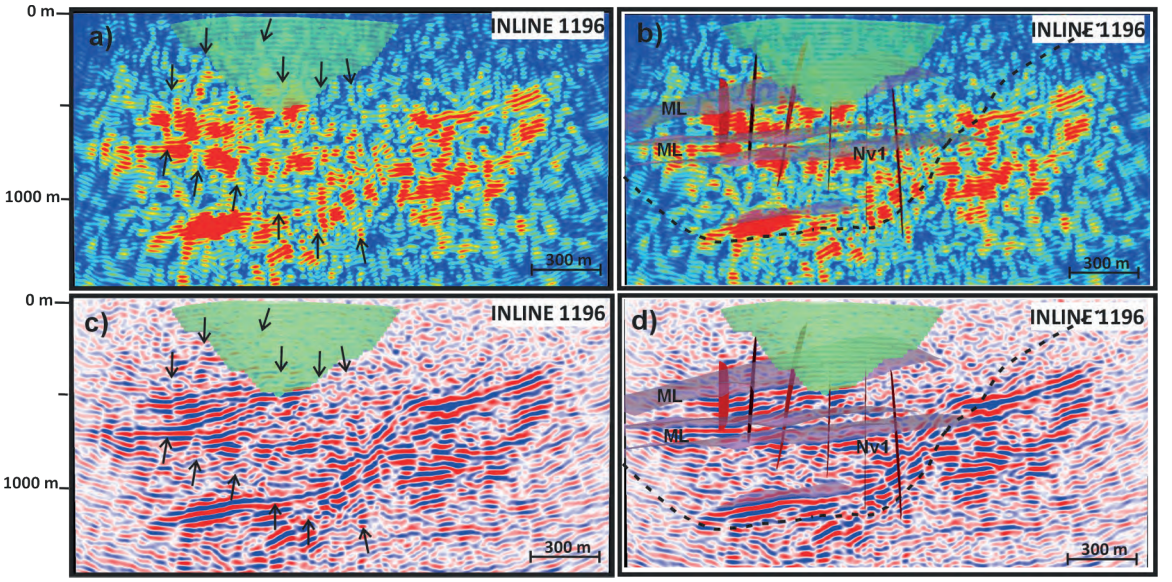


**Figure 5.** Inline 1196 of the a-b) amplitude envelope and c-d) seismic amplitude attribute of the 3D seismic data (migrated; Malehmir et al. 2012b). Viewed from east. The planned open pit shown in green as a reference. Internal reflectivity, earlier (Koivisto et al. 2015) interpreted to represent contacts between magmatic layers (ML), is shown in b) and d). Black arrows indicate the locations of the interpreted near vertical structure that are shown on b) and d). In total nine new structures were interpreted in the inline sections of the 3D seismic data of which six are shown on this figure. NV1 (location shown in b) and d)) was the only near vertical structure in the inline direction modelled by Koivisto et al. (2015). However, it also seems more continuous on the amplitude envelope attribute display and, therefore, it has been extended in the updated 3D model of near mine structures. The black dashed line (in b) and d)) indicates the approximate intersection of the base of the intrusion (Koivisto et al. 2015) and inline 1196. The depth is referenced to the datum level of the 3D seismic reflection data (at 290 m above sea level).

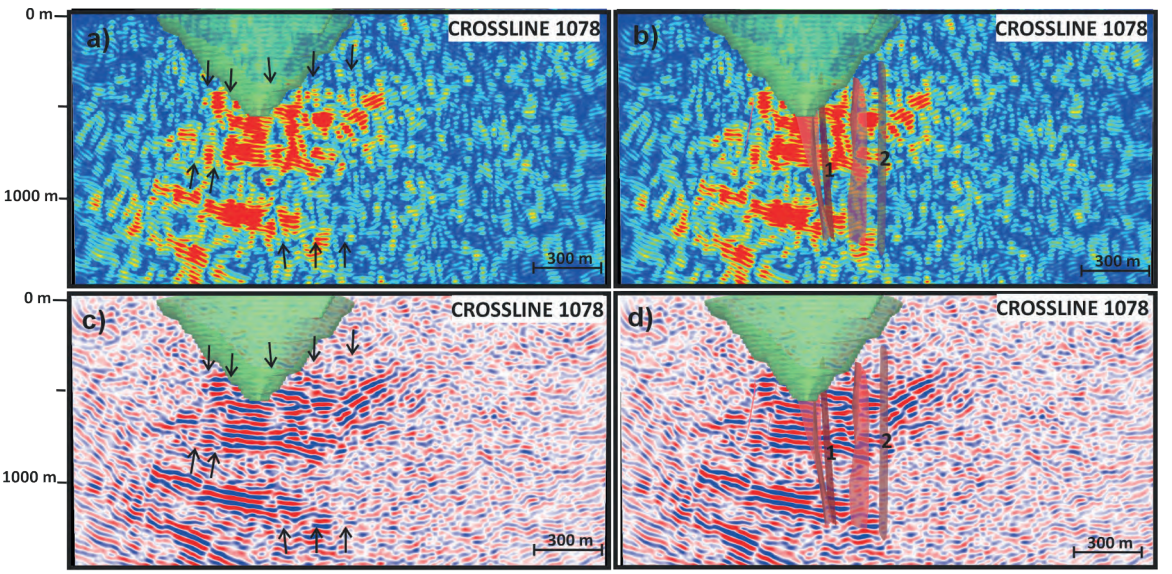


**Figure 6**. Crossline 1078 of the a-b) amplitude envelope and c-d) seismic amplitude attribute of the 3D seismic data (migrated; Malehmir et al. 2012b). Viewed from north. The planned open pit (green) shown as a reference. Black arrows indicate the locations of the interpreted near vertical structure that are shown on b) and d). One new structure (labeled as 1 in the figure) was interpreted in the crossline sections of the 3D seismic data. In addition, near vertical structures NV4 and NV6 modeled by Koivisto et al. (2015) seem to have connection in the amplitude envelope display. A new structure (labeled as 2 in the figure) that merge and extends the NV4 and NV6 was modelled. The depth is referenced to the datum level of the 3D seismic reflection data (at 290 m above sea level).

discontinuities or breaks seemed to align well in different attribute displays. However, the near-vertical structures seemed more continuous. In addition, several new near-vertical structures, especially in inline direction, were observed within the internally reflective part of the intrusion. In total nine new near-vertical structures were interpreted in the inline sections of the 3D seismic data (some of which are shown in Fig. 5). There was only one near-vertical structure (NV1) in the inline direction in the previous model by Koivisto et al. (2015). However, NV1 also seems more continuous on the amplitude envelope attribute display and, therefore, it was extended. In the crossline direction, one new near-vertical structure was identified (marked as 1 in Fig. 6). In addition, near-vertical structures NV4 and NV6 modeled by Koivisto et al. (2015) seemed to have connection in the amplitude envelope display. Therefore, a new structure (marked as 2 in Fig. 6) was modelled that merged and extended the NV4 and NV6.

# 5. Discussion

## *5.1. Comparison of seismic attributes with modelled lithological contacts and near mine structures*

Comparison of the calculated seismic attributes with the modelled lithological contacts and near mine structures by Koivisto et al. (2015) is illustrated in Fig. 3–8. In general, similar reflectivity is observed within the different attribute displays of the Kevitsa 3D seismic data (Fig. 3–8). Particularly, the modelled lithological contacts by Koivisto et al. (2015), such as the base of the intrusion, seem to align well in different attribute displays. However, in the calculated seismic attribute displays, e.g., amplitude envelope display, some of the modelled structures (Koivisto et al. 2015) seem more continuous, and in places, they seem to penetrate the whole Kevitsa resource area where the internal reflectivity is observed. In the Kevitsa 3D seismic data, the reflectivity is observed as packages of reflections rather than a single reflector as also noted earlier (e.g., Malehmir et al. 2012b; Koivisto et al. 2012, 2015; Junno et al. 2020). The seismic attribute analysis, especially amplitude envelope display shown in Fig. 5–8, have enhanced the observability of the discontinuity of these reflective packages. The internal reflectivity, earlier interpreted to represent magmatic layering (ML in Figs. 5 and 7 modeled by Koivisto et al. 2015) within the intrusion, seem to consist of several smaller reflective packages that have clear breaks in between rather than horizontally continuous reflective package. Therefore, the amplitude envelope attribute seems to delineate the reflective areas more precisely. Junno et al. (2020) interpreted alteration and possibly associated mineralization as plausible cause for the observed internal reflectivity. Enhanced delineation of the internal reflective packages can be significant for the mineral exploration purposes at depth. In addition, new features (discontinuities or breaks in reflectivity) are observed in the seismic attribute displays within the Kevitsa intrusion near the open pit mine that could represent additional structures (Figs. 5 and 6). These new structures can potentially be critical for geotechnical planning of the Kevitsa open pit.

Fig. 7 presents the inline 1157 (see location in Fig. 1) of the 3D seismic data with seismic amplitude in Fig. 7a and 7b and amplitude envelope display in Fig. 7c and 7d. Several surfaces representing modelled lithological contacts (base of the Kevitsa intrusion (BK), earlier interpreted magmatic layering (ML)) and near mine structures (R8 (see details below) and I5 and I9) are shown in Fig. 7b and 7d on top of the 3D seismic data as an example (based on Koivisto et al. 2015). Black arrows in Fig. 7a and 7c indicate the locations of these interpreted surfaces. Reflector R8 (see details in Malehmir et al. 2012b; Koivisto et al. 2015; Lindqvist et al. 2017; Malehmir et al. 2018) is observed in the seismic data as a reflector but it is classified as a structure as it offsets other reflectors. R8 forms a boundary that divides the intrusion to

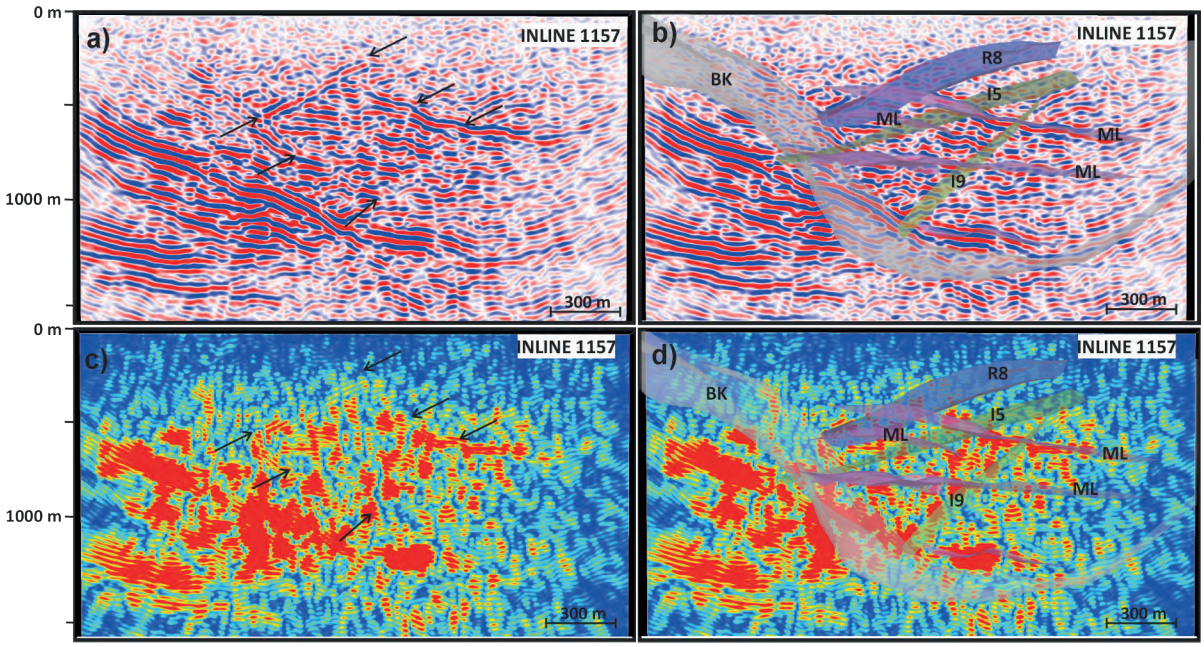


**Figure 7.** Inline 1157 of the a-b) seismic amplitude and c-d) amplitude envelope attribute of the 3D seismic data (migrated; Malehmir et al. 2012b). Viewed from west. The base of the Kevitsa intrusion (BK; Koivisto et al. 2015) shown as a reference in b) and d). Black arrows indicate the locations of the interpreted structures (R8, I5 and I9 (inline structure)). Internal reflectivity, earlier interpreted to represent contacts between magmatic layers (ML), is shown in b) and d). Generally, the same features as observed in both attributes. However, the reflective packages seem more clearly horizontally discontinuous in amplitude envelope attribute display. Figure is based on Koivisto et al. (2015). The depth is referenced to the datum level of the 3D seismic reflection data (at 290 m above sea level).

internally reflective and non-reflective areas and it can be followed to shallower depths than other structures (150–200 m depth; Fig. 7). Reflector R8 is interpreted to represent a major fracture zone extending to 600 m depth and 1000 m laterally. In addition to its importance to pit stability, this zone controls the extent of the economic mineralization in Kevitsa (Malehmir et al. 2018). The known mineralization lies east of the reflector R8.

Fig. 8 presents the crossline 1111 (see location in Fig. 1) of the 3D seismic data with seismic amplitude in Fig. 8a and 8b and amplitude envelope display in Fig. 8c and 8d. Also, in this figure several surfaces (C2, C6 and C8 representing larger discontinuities in crossline direction, and NV3 and NV4 as smaller scale, near-vertical structures) are shown as an example of the model by Koivisto et al. (2015). These figures highlight the discontinuity of the reflections in the amplitude envelope display.

## *5.2. Implications for the potential cause of the internal reflectivity within the Kevitsa intrusion*

Seismic attribute analysis has become a crucial tool in interpretation of seismic data in hard rock environments (e.g., Stuart et al. 2000; Manzi et al. 2012, 2013, 2020; Hale 2013; Nkosi et al. 2018; Zhang & Wang 2024). For example, seismic attribute analysis has improved the quality and efficiency of fault detection in 3D seismic data and been used to successfully image structures that were seismically transparent in the amplitude display (e.g., Nkosi et al. 2018). In addition, the attributes have improved the lateral continuity of structures and aided in determination of the fault continuity and cross relationships (Nkosi et al. 2018). The amplitude envelope attribute, in particular, is useful in highlighting steeply dipping discontinuities and faults that are usually

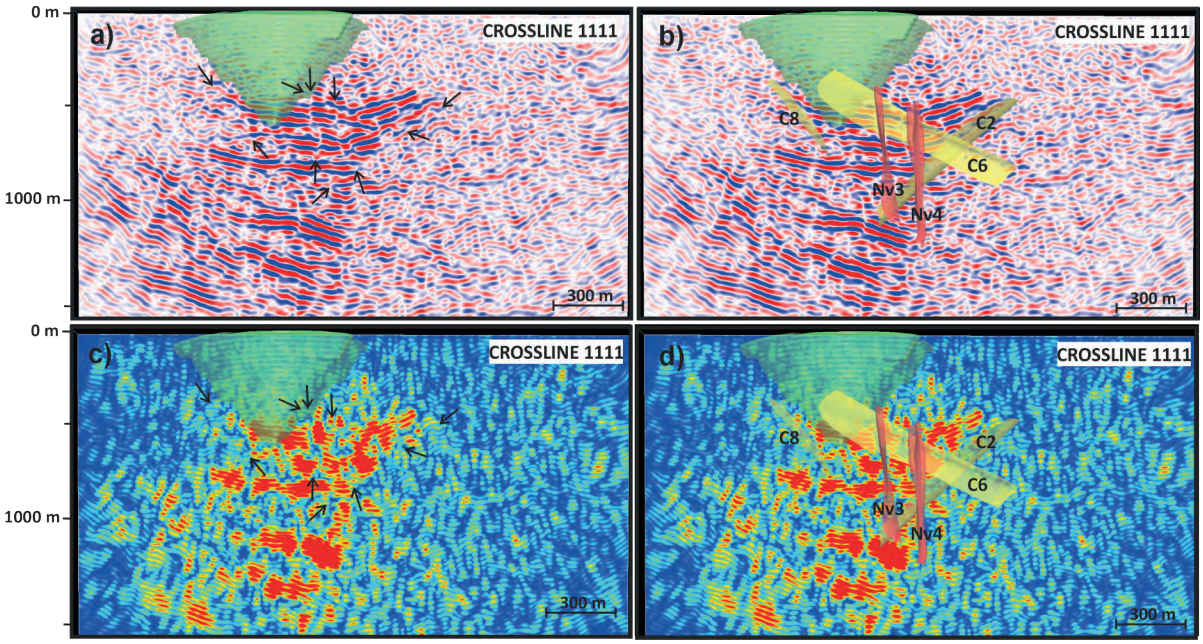


**Figure 8.** Crossline 1111 of the a-b) seismic amplitude and c-d) amplitude envelope attribute of the 3D seismic data (migrated; Malehmir et al. 2012b). Viewed from north. The planned open pit shown in green as a reference. Black arrows indicate the locations of the interpreted structures in crossline direction near the close vicinity of the planned open pit (C2, C6, C8 (crossline structure), NV3, NV4 (near vertical structure) modelled by Koivisto et al. 2015). The amplitude envelope attribute display indicates the same structures as the seismic amplitude, however, showing slightly higher fidelity and confirming the existence of the structures. Figure is based on Koivisto et al. (2015). The depth is referenced to the datum level of the 3D seismic reflection data (at 290 m above sea level).

characterized by laterally discontinuous features within the amplitude envelope display. Based on the seismic attribute analysis of the Kevitsa 3D seismic data, the 3D model of near mine structures by Koivisto et al. (2015) was updated. Some of the modelled structures (Koivisto et al. 2015) within the Kevitsa intrusion seem more continuous in the amplitude envelope display, and in places, they seem to penetrate the whole Kevitsa resource area where the internal reflectivity is observed. In addition, new features that could represent additional structures are observed within the resource area using seismic attribute analysis. These later structures cut the originally continuous internal reflectors into piecewise packages. Better understanding of the spatial distribution of these reflective packages can be significant for targeted mineral exploration at depth and the structures can potentially be critical for geotechnical planning of the Kevitsa open pit at greater depths.

Some fracture and fault zones may also appear reflective within the seismic data. It has been suggested that this enhanced reflectivity may be characteristic of structures that were conduits for hydrothermal and potentially mineralizing fluids (Dentith & Mudge 2014). Alteration has been interpreted in many papers to affect the seismic properties and observed reflectivity in seismic data (e.g., Chopping 2008; Heinonen et al. 2012; Miah et al. 2015; Schetselaar et al. 2019; de Souza et al. 2020; Junno et al. 2020). Alteration caused by hydrothermal fluid-flow through a fault zone is therefore a possible cause of acoustic impedance contrast. As in the case of the Kevitsa seismic data, structure R8 is observed as reflective rather than none-reflective feature, and it has been interpreted as a fracture zone (e.g., Malehmir et al. 2018). The reflector R8 is the most significant fracture zone at deeper levels, and it can be traced through several inlines of the reflection volume (Koivisto et al.

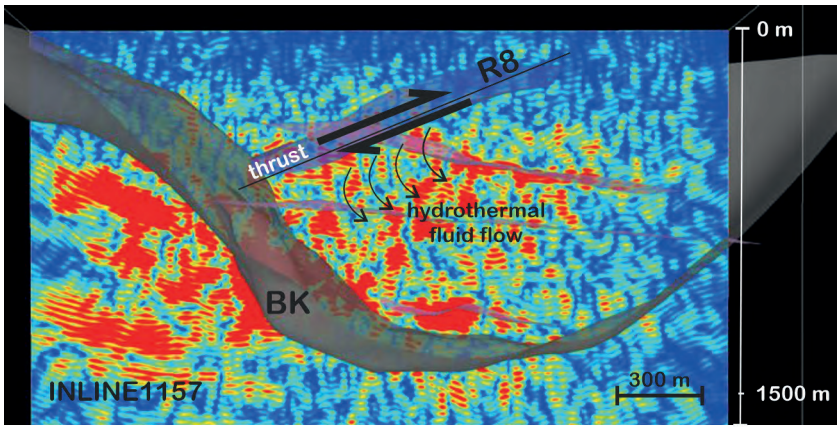


**Figure 9.** Inline 1157 of the amplitude envelope attribute of the 3D seismic data (migrated; Malehmir et al. 2012b). Viewed from west. The base of the Kevitsa intrusion (BK; Koivisto et al. 2015) shown as a reference. Surface R8, shown in purple, is interpreted to represent major NE-striking trust fault, which acted as a pathway for hydrothermal fluids that enable alteration, and possible mineralization, within the Kevitsa intrusion. Alteration, and possibly associated mineralization, is observed as internal reflectivity within the intrusion (Junno et al. 2020). The depth is referenced to the datum level of the 3D seismic reflection data (at 290 m above sea level).

2015), and all the way to the open pit (Lindqvist et al. 2017). In general, it has been suggested that enhanced reflectivity may be characteristic of structures that were conduits for hydrothermal and potentially mineralizing fluids (e.g., Dentith & Mudge 2014; Schetselaar et al. 2019). Alteration caused by hydrothermal fluid-flow through a fault zone is therefore possible cause of an acoustic impedance contrast. Malehmir et al. (2018) interpreted R8 as a thrust sheet that possibly acted as a conduit for hydrothermal fluid circulations within the Kevitsa intrusion. Reflector R8 forms a boundary that divides the Kevitsa intrusion to internally reflective and non-reflective parts. The internally reflective part of the intrusion is associated with the economic mineralization, and hence, R8 defines a major boundary for the extent of economic mineralization and might have acted as a key structure in redistributing economic mineralization within the Kevitsa intrusion (Fig. 9).

The reflector R8 seem to be associated with negative reflection polarity, whereas the observed internal reflectivity has a positive polarity. Negative polarity reflects the change from higher petrophysical (velocity, density) properties to lower properties. Based on results by Junno et al. (2020) this could indicate increasing alteration within the thrust sheet (i.e., R8) compared to surroundings. Although, brittle, low RQD rocks (i.e., fracture zone) would also be associated with lower petrophysical properties. Based on the field photos (Lindqvist et al. 2017; Malehmir et al. 2018), R8 is a highly brittle, weathered, and oxidized zone. Closer look at the borehole data showed that more than 35 boreholes cut the modelled surface interpreted to represent reflector R8. The lithology logged for these boreholes at the level they cut R8 is olivine pyroxenite or metaperidotite. Metaperidotite refers to various degrees of amphibole alteration of olivine pyroxenites. In addition, moderate to intense amphibole alteration is logged at the intersection level. Some of these boreholes also indicate increased levels of disseminated pyrrhotite and chalcopyrite. These observations would support the hypothesis that R8 acted as a conduit for hydrothermal fluids that enabled alteration and possibly also mineralization within the Kevitsa intrusion.

### 5.3. Genetic implications deduced from seismic data

Our results imply a set of constraints for the ore genesis at the Kevitsa deposit. We suggest a genetic link between the observed internal reflectivity and earlier suggested magmatic layering, country rock contamination, hydrothermal alteration and sulfide mineralization. Junno et al. (2020) showed that hydrothermal alteration of the ultramafic rocks was necessary in generating the seismic reflectivity in the Kevitsa intrusion. Lithological variation or sulfide content alone are not able to explain the observed change in acoustic impedance and, hence, reflectivity. However, the sulfide content was found to have a possible link to the alteration. The existence of several seismically reflective layers within a restricted region inside the Kevitsa intrusion – associated with the Kevitsa resource area – can be attributed to successive magma pulses affected by country rock contamination and hydrothermal alteration which is suggested to have more pervasively affected the more olivine- and clinopyroxene-rich bases of the pulses. After the initial formation of the larger-scale intrusion, more successive magma pulses intruded into the region around the current Kevitsa resource area, constrained by the reflector R8 and the Central Dunite (Fig. 1; Luolavirta et al. 2018a, 2018c), through a different route involving country rock contamination and/or a collapse of the roof of the magma chamber may have taken place at this point of the process, also introducing volatiles to the system to aid hydrothermal alteration. Our observations support the earlier presented genetic models by Mutanen (1997, 2005) and Luolavirta et al. (2018c). The hydrothermal alteration may have been further aided by introduction of water through structures such as R8 (borehole data indicate the presence of metaperidotite, i.e., amphibole altered olivine pyroxenites, along this zone). The reflective layers are subhorizontal and the orientation follows the footwall contact of the intrusion supporting a magmatic origin. Overall, our interpretation is that the reflective layers represent altered and possibly mineralized (sulfide-bearing) parts of the magma pulses. At later stages when the intrusion was already solidified but still hot, shearing resulted in the structures cross-cutting the magmatic layering into piece-wise packages as suggested by the seismic data (Figs. 5 and 7), allowing fluid flow through them which resulted in hydrothermal alteration of some of these structures as well (Gervilla & Kojonen 2002; Le Vaillant et al. 2016). These later processes may have involved further remobilization of sulfides.

The currently available drilling data, alteration mapping and wireline logging of seismic impedances do not yet allow testing the hypothesis in detail. However, our results can be applied as a working hypothesis in resource mapping in the mine scale and reconstruction of the magma chamber, magmatic layers, alteration and cross-cutting structures with 3D seismic data.

## 6. Conclusions

In summary from above, we draw the following conclusions:

1. In addition to the previously interpreted lithological contacts and structures, the seismic attribute analysis of the Kevitsa 3D seismic data revealed more details of the internal structure of the Kevitsa intrusion.
2. We attribute the existence of several subhorizontal seismically reflective layers within the Kevitsa resource area to successive magma pulses affected by country rock contamination and hydrothermal alteration. The reflective layers represent altered and possibly mineralized parts of the successive magma pulses.
3. The internal reflectors within the intrusion appear more discontinuous in the amplitude envelope displays compared to the conventional seismic amplitude display. This enhanced delineation of the reflective packages is potentially significant for targeted mineral exploration at depth.

4. We suggest that R8 – a reflective structure that divides the intrusion into internally reflective and non-reflective areas – acted as a barrier for the creation of the Kevitsa resource area as well as a pathway for hydrothermal fluids that aided alteration, and possibly also the mineralization, within the Kevitsa resource area.
5. The seismic attribute analysis allows to interpret new near mine structures not seen in the conventional amplitude display. Some of the modelled structures (Koivisto et al. 2015) seem more continuous, and in places, they seem to penetrate the whole Kevitsa resource area where the internal reflectivity is observed. These interpreted later structures have cut originally continuous internal reflectors into piecewise packages. These structures can potentially be critical for geotechnical planning of the Kevitsa open pit at greater depths.

## Acknowledgements

This research was initially funded through a grant from K. H. Renlund Foundation to the first author. The authors would like to thank Boliden AB for their collaboration and data. Paradigm GOCAD® and Mira Geoscience Ltd. GODAC® Mining Suite provided an academic license used for 3D visualization and interpretation of the seismic data, as well as for seismic attribute analysis and updating and building the 3D model of the near mine structures (surfaces). We thank Dr Tuomo Karinen and two anonymous reviewers along with the editors, Jussi S. Heinonen and Suvi Heinonen for their useful comments that improved the quality of our work and presentations.

## Authorship contribution statement

N. Junno – analytical work, background, conceptualization, interpretation, modeling, visualization, writing; E. Koivisto – conceptualization, editing, interpretation, writing; I. Kukkonen – editing, interpretation, writing.

## References

Adam, E., Perron, G., Arnold, G., Matthews, L & Milkereit, B., 2003. 3D seismic imaging for VMS deposit exploration, Matagami, Quebec. In: Eaton, D. W. et al. (eds.), Hardrock seismic exploration, Society of Exploration Geophysicists, pp. 229–246. https://doi.org/10.1190/1.9781560802396.ch15

Alcalde, J., Carbonell, R., Pospiech, S., Gil, A., Bullock, L. A. & Tornos, F., 2022. Preface: State of the art in mineral exploration, Solid Earth 13, 1161–1168. https://doi.org/10.5194/se-13-1161-2022.

Bellefleur, G., Malinowski, M. & Urosevic, M., 2019. Editorial for Special Issue "Seismic Methods in Mineral Exploration", Minerals 9, 630. https://doi.org/10.3390/min9100630

Berthet, L., 2024. Boliden Summary Report, Resources and Reserves 2023. Kevitsa Mine. Boliden AB.

Boliden AB., 2024. Boliden annual and sustainability report 2023. www.boliden.com

Chopping, R., 2008. Geophysical signatures of alteration. Project A3 Final Report. Predictive Mineral Discovery Cooperative Research Centre, Geoscience Australia.

Dentith, M. & Mudge, S. T., 2014. Geophysics for the mineral exploration geoscientist. Cambridge University Press, 454 p. https://doi.org/10.1017/CBO9781139024358

Dewett, D. T., Pigott, J. D. & Marfurt, K. J., 2021. A review of seismic attribute taxonomies, discussion of their historical use, and presentation of a seismic attribute communication framework using data analysis concepts. Interpretation 9, B39–B64. https://doi.org/10.1190/INT-2020-0222.1

Drummond, B.J., Goleby, B.R., Goncharov, A.G., Wyborn, L.A.I. & MacCready, T., 1998. Crustal-scale structures in the Proterozoic Mount Isa Inlier of north Australia: Their seismic response and influence on mineralization. Tectonophysics 288, 43–56. https://doi.org/10.1016/S0040-1951(97)00282-5

Gervilla, F. & Kojonen, K., 2002. The platinum-group minerals in the upper section of the Keivitsansarvi Ni-Cu-PGE deposit, northern Finland. The Canadian Mineralogist 40, 377–394. https://doi.org/10.2113/gscanmin.40.2.377

Gregory, J., Journet, N., White, G. & Lappalainen, M., 2011. Kevitsa Copper Nickel Project Finland: NI 43-101 Technical Report for the Mineral Resources and Reserves of the Kevitsa Project. First Quantum Minerals Ltd.

Hale, D., 2013. Methods to compute fault images, extract fault surfaces, and estimate fault throws from 3D seismic images. Geophysics 78, O33–O43. https://doi.org/10.1190/geo2012-0331.1

Hanski, E., Huhma, H. & Vaasjoki, M., 2001. Geochronology of northern Finland: a summary and discussion. In: Vaasjoki, M. (ed.) Radiometric age determinations from Finnish Lapland and their bearing on the timing of Precambrian volcano-sedimentary sequences. Geological Survey of Finland Special Paper 33, 255–279. http://tupa.gtk.fi/julkaisu/specialpaper/sp_033.pdf

Hanski, E. & Huhma, H., 2005. Central Lapland greenstone belt. In: Lehtinen, M. et al. (eds.), Precambrian geology of Finland – Key to the evolution of the Fennoscandian Shield. Elsevier, Amsterdam, pp. 139–194. https://doi.org/10.1016/S0166-2635(05)80005-2

Heinonen, S., Imana, M., Snyder, D.B., Kukkonen, I.T. & Heikkinen, P., 2012. Seismic reflection profiling of the Pyhäsalmi VHMS-deposit: a complementary approach to the deep base metal exploration in Finland. Geophysics 77, WC15–WC23. https://doi.org/10.1190/geo2011-0240.1

L'Heureux, E., Milkereit, B. & Vasudevan, K., 2009. Heterogeneity and seismic scattering in exploration environments. Tectonophysics 472, 264–272. https://doi.org/10.1016/j.tecto.2008.04.001

Huhma, H., Hanski, E., Kontinen, A., Vuollo, J., Mänttäri, I. & Lahaye, Y., 2018. Sm-Nd and U-Pb isotope geochemistry of the Palaeoproterozoic mafic magmatism in eastern and northern Finland. Geological Survey of Finland, Bulletin 405, 150 p. https://tupa.gtk.fi/julkaisu/bulletin/bt_405.pdf

Junno, N., Koivisto, E., Kukkonen, I., Malehmir, A., Wijns, C. & Montonen, M., 2020. Data mining of petrophysical and lithogeochemical borehole data to elucidate the origin of seismic reflectivity within the Kevitsa Ni-Cu-PGE –bearing intrusion, northern Finland. Geophysical Prospecting 68, 82–102. https://doi.org/10.1111/1365-2478.12907

Koivisto, E., Malehmir, A., Heikkinen, P., Heinonen, S. & Kukkonen, I., 2012. 2D seismic reflection investigations at the Kevitsa Ni-Cu-PGE deposit, northern Finland. Geophysics 77, pp. WC149–WC162. https://doi.org/10.1190/geo2011-0496.1

Koivisto, E., Malehmir, A., Hellqvist, N., Voipio, T. & Wijns, C., 2015. Building a 3D model of lithological contacts and near-mine structures in the Kevitsa mining and exploration site, northern Finland. Geophysical Prospecting 63, 754–773. https://doi.org/10.1111/1365-2478.12252

Kukkonen, I., Lahti, I., Heikkinen, P. & HIRE Working Group of the Geological Survey of Finland, 2009. HIRE Seismic Reflection Survey in the Kevitsa Ni-PGE deposit, North Finland. Geological Survey of Finland, Report Q23/2008/59.

Labrunye, E. 2004. Extraction automatique d'information géologique à partir d'images sismiques tridimensionnelles. Doctoral dissertation, Institut National Polytechnique de Lorraine. 150 p.

Lamberg, P., Välimaa, J., Parkkinen, J. & Kojonen, K., 2005. Structural, geochemical and magmatic modelling of the early Proterozoic Keivitsa Ni-Cu-PGE deposit in Sodankylä, northern Finland. In: Törmänen, T. & Alapieti, T. (ed.), Platinum-Group Elements – From Genesis to Beneficiation and Environmental Impact - Extended Abstracts, pp. 160–163.

Lindqvist, T., Skyttä, P., Koivisto, E., Häkkinen, T. & Somervuori, P., 2017. Delineating the network of brittle structures with geotechnical, structural and reflection seismic data, Kevitsa open pit, Northern Finland. GeoResJ 13, 159–174. https://doi.org/10.1016/j.grj.2017.04.004

Le Vaillant, M., Barnes, S. J., Fiorentini, M.L., Santaguida, F. & Törmänen, T., 2016. Effects of hydrous alteration on the distribution of base metals and platinum group elements within the Kevitsa magmatic nickel sulphide deposit. Ore Geology Reviews 72, 128–148. https://doi.org/10.1016/j.oregeorev.2015.06.002

Le Vaillant, M., Hill, J. & Barnes, S., 2017. Simplifying Drill-Hole Domains For 3D Geochemical Modelling: An Example From The Kevitsa Ni-Cu-(PGE) Deposit. Ore Geology Reviews 90, 388–398. https://doi.org/10.1016/j.oregeorev.2017.05.020

Luolavirta K., Hanski E., Maier W. & Santaguida F., 2018a. Characterization and origin of dunitic rocks in the Ni-Cu sulphide-bearing Kevitsa intrusion: whole-rock and mineral compositional constrains. Bulletin of the Geological Society of Finland 90, 5–32. https://doi.org/10.17741/bgsf/90.1.001

Luolavirta, K., Hanski, E., Maier, W. & Santaguida, F., 2018b. Whole-rock and mineral compositional constraints on the magmatic evolution of the Ni-Cu-(PGE) sulfide ore-bearing Kevitsa intrusion, northern Finland. Lithos 269–299, 37–53. https://doi.org/10.1016/j.lithos.2017.10.015

Luolavirta, K., Hanski, E., Maier, W., Lahaye, Y., O'Brien, H. & Santaguida, F., 2018c. In situ strontium and sulfur isotope investigation of the Ni-Cu-(PGE) sulfide ore-bearing Kevitsa intrusion, northern Finland. Mineralium Deposita 53, 1019–1038. https://doi.org/10.1007/s00126-018-0792-6

Malehmir, A. & Bellefleur, G. 2009. 3D seismic reflection imaging of volcanic-hosted massive sulfide deposits: Insights from reprocessing of the Halfmile Lake data, New Brunswick, Canada: Geophysics 74, B209–B219. https://doi.org/10.1190/1.3230495

Malehmir, A., Durrheim, R., Bellefleur, G., Urosevic, M., Juhlin, C., White, D. J., ... & Campbell, G., 2012a.

Seismic methods in mineral exploration and mine planning: A general overview of past and present case histories and a look into the future. Geophysics, 77, WC173–WC190. https://doi.org/10.1190/geo2012-0028.1

Malehmir, A., Juhlin, C., Wijns, C., Urosevic, M., Valasti, P. & Koivisto, E., 2012b. 3D seismic reflection imaging for open-pit mine planning and deep exploration in the Kevitsa Ni-Cu- PGE deposit, northern Finland. Geophysics 77, WC95–WC108. https://doi.org/10.1190/geo2011-0468.1

Malehmir, A., Koivisto, E., Manzi, M., Cheraghi, S., Durrheim, R.J., Bellefleur, G., Wijns, C., Hein, K.A.A. & King, N., 2014. A review of seismic reflection investigations in three major metallogenic regions: The Kevitsa Ni-Cu-PGE (Finland), Witwatersrand goldfields (South Africa), and the Bathurst Mining Camp (Canada). Ore Geology Reviews 56, 423–441. https://doi.org/10.1016/j.oregeorev.2013.01.003

Malehmir, A., Durrheim, R., Bellefleur, G., Urosevic, M., Juhlin, C., White, D.J., Milkereit, B. & Campbell, G., 2015. Seismic methods in mineral exploration and mine planning: a general overview of past and present case histories and a look into the future. Geophysics, 77, WC173–WC190. https://doi.org/10.1190/geo2012-0028.1

Malehmir, A., Tryggvason, A., Wijns, C., Koivisto, E., Lindqvist, T., Skyttä, P. & Montonen, M., 2018. Why 3D seismic data are an asset for exploration and mine planning? Velocity tomography of weakness zones in the Kevitsa Ni-Cu-PGE mine, northern Finland. Geophysics 83, B33–B46. https://doi.org/10.1190/geo2017-0225.1

Malehmir, A., Manzi, M., Draganov, D., Weckmann, U. & Auken, E., 2020. Introduction to the special issue on "Cost-effective and innovative mineral exploration solutions". Geophysical Prospecting 68, 3–6. https://doi.org/10.1111/1365-2478.12915

Malehmir, A., Markovic, M., Marsden, P., Gil, A., Buske, S., Sito, L., Bäckström, E., Sadeghi, M. & Luth, S., 2021. Sparse 3D reflection seismic survey for deep-targeting iron oxide deposits and their host rocks, Ludvika Mines, Sweden. Solid earth, 12, 483–502. https://doi.org/10.5194/se-12-483-2021

Mallet J.L. 1997. Discrete modelling for natural objects. Journal of Mathematical Geology 29, 199–219. https://doi.org/10.1007/BF02769628

Manzi, M. S. D., Durrheim, R. J., Hein, K. A. A. & King, N., 2012. 3D edge detection seismic attributes used to map potential conduits for water and methane in deep gold mines in the Witwatersrand basin, South Africa. Geophysics 77, WC133–WC147. https://doi.org/10.1190/geo2012-0135.1

Manzi, M. S. D., Hein, K. A. A., Durrheim, R. & King, N., 2013. Seismic attribute analysis to enhance detection of thin gold-bearing reefs: South Deep gold mine, Witwatersrand basin, South Africa. Journal of Applied Geophysics 98, 212–228. https://doi.org/10.1016/j.jappgeo.2013.08.017

Manzi, M., Copper, G. R. J., Malehmir, A. & Durrheim, R. J., 2020. Improved structural interpretation of legacy 3D seismic data from Karee platinum mine (South Africa) through the application of novel seismic attributes. Geophysical Prospecting 68, 145–163. https://doi.org/10.1111/1365-2478.12900

Miah, K. H., Bellefleur, G., Schetselaar, E. & Potter, D. K., 2015. Seismic properties and effects of hydrothermal alteration on Volcanogenic Massive Sulfide (VMS) deposits at the Lalor Lake in Manitoba, Canada. Journal of Applied Geophysics 123, 141–152. https://doi.org/10.1016/j.jappgeo.2015.07.016

Milkereit, B., Eaton D.W., Wu J., Perron G., Salisbury M.H., Berrer E. & Morrison G., 1996. Seismic imaging of massive sulphide deposits: Part II. Seismic reflection profiling. Economic Geology 91, 829–834. https://doi.org/10.2113/gsecongeo.91.5.829

Mutanen, T., 1997. Geology and ore petrology of the Akanvaara and Koitelainen mafic-layered intrusions and the Keivitsa-Satovaara layered complex, northern Finland. Bulletin of the Geological Survey of Finland 395, 233 p.

Mutanen, T. & Huhma, H., 2001. U-Pb geochronology of the Koitelainen, Akanvaara and Keivitsa mafic layered intrusions and related rocks. In: Vaasjoki, M. (ed.), Radiometric Age Determinations from Finnish Lapland and Their Bearing on the Timing of Precambrian Volcano-Sedimentary Sequences. Geological Survey of Finland, Special Paper 33, pp. 229–246.

Mutanen, T., 2005. Field Trip Guide: Akanvaara intrusion and the Keivitsa-Satovaara complex, with stops at Kaikkivaltiaanlehto and Rantavaara intrusions. Geological Survey of Finland, Guide 51b.

Nkosi, N. Z., Manzi, M. S., Brovko, O., & Durrheim, R. J., 2018. 3D seismic attributes for structural mapping and enhancement of deep gold mining: a case study from the West Wits Line goldfields, South Africa. Exploration Geophysics 49, 345–362. https://doi.org/10.1071/EG16058

Pittuck, M. & Lepley, B., 2019. Technical report for the Kevitsa Cu-Ni-PGE mine, Finland. Boliden Kevitsa Mining Oy. https://www.boliden.com/globalassets/operations/exploration/mineral-resources-and-mineral-reserves-pdf/2019/resources_and_reserves_kevitsa_technical_report_2019-12-31.pdf

Salisbury, M., Harvey C.W. & Matthews L., 2003. The acoustic properties of ores and host rocks in hardrock terranes. In: Eaton, D. et al. (eds.), Hardrock seismic exploration. SEG, pp. 9–19. https://doi.org/10.1190/1.9781560802396.ch1

Santaguida, F., Luolavirta K., Lappalainen M., Ylinen J., Voipio T. & Jones S., 2015. The Kevitsa Ni-Cu-PGE deposit in the Central Lapland Greenstone Belt in Finland. In:

Maier, W.D. et al. (eds), Mineral Deposits of Finland. Elsevier, pp. 195–210. https://doi.org/10.1016/B978-0-12-410438-9.00008-X

Schetselaar, E., Bellefleur, G. & Hunt, P., 2019. Elucidating the effects of hydrothermal alteration on seismic reflectivity in the footwall of the Lalor Volcanogenic Massive Sulfide Deposit, Snow Lake, Manitoba, Canada. Minerals 9, 384. https://doi.org/10.3390/min9060384

de Souza, A. E. C. M. & Vialle, S., 2020. Understanding seismic reflectivity across hydrothermal alteration zones associated with gold: Example of the Karari gold deposit, Western Australia. Ore Geology Reviews 126, 103776. https://doi.org/10.1016/j.oregeorev.2020.103776

Standing, J., De Luca, K., Outhwhaite, M., Lappalainen, M., Wijns, C., Jones, S. et al., 2009. Report and Recommendations from the Kevitsa Campaign, Finland. Confidential Report to First Quantum Minerals Ltd. Jigsaw Geosciences Pty Ltd., West Perth, Australia, 125 p.

Stuart, G. W., Jolley, S. J., Polome, L. G. & Tucker, R. F., 2000. Application of 3-D seismic attributes analysis to mine planning Target gold deposit, South Africa. The Leading Edge 19, 736–742. https://doi.org/10.1190/1.1438706

Taner, M.T., Koehler, F. & Sheriff, R.E., 1979. Complex seismic trace analysis. Geophysics 44, 1041–1063. https://doi.org/10.1190/1.1440994

Taner, M. T., 2001. Seismic Attributes. CSEG Recorder, pp. 48–56.

Yang, S., Maier, W., Hanski, E., Lappalainen, M., Santaguida, F. & Määttä, S., 2013. Origin of ultra-nickeliferous olivine in the Kevitsa Ni–Cu–PGE-mineralized intrusion, northern Finland. Contributions to Mineralogy and Petrology 166, 81–95. https://doi.org/10.1007/s00410-013-0866-5.

Zhang, B. & Wang, Y., 2024. Seismic attribute-assisted seismic fault interpretation. Geophysics 89, N1–N13. https://doi.org/10.1190/geo2023-0060.1